fractal and fractional

MDPI

Article

Optimal Fractional-Order Controller for the Voltage Stability of a DC Microgrid Feeding an Electric Vehicle Charging Station

Sherif A. Zaid [1,*], Abualkasim Bakeer [2], Hani Albalawi [1,3], Aadel M. Alatwi [1,4], Hossam AbdelMeguid [5,6] and Ahmed M. Kassem [7]

1 Electrical Engineering Department, Faculty of Engineering, University of Tabuk, Tabuk 47913, Saudi Arabia
2 Department of Electrical Engineering, Faculty of Engineering, Aswan University, Aswan 81542, Egypt; abualkasim.bakeer@aswu.edu.eg
3 Renewable Energy & Energy Efficiency Centre (REEEC), University of Tabuk, Tabuk 47913, Saudi Arabia
4 Industrial Innovation and Robotic Center (IIRC), University of Tabuk, Tabuk 47731, Saudi Arabia
5 Department of Mechanical Engineering, Faculty of Engineering, University of Tabuk, Tabuk 47913, Saudi Arabia
6 Mechanical Power Engineering Department, Faculty of Engineering, Mansoura University, El-Mansoura 35516, Egypt
7 Electrical Engineering Department, Faculty of Engineering, Sohag University, Sohag 82524, Egypt
* Correspondence: shfaraj@ut.edu.sa

Abstract: Charging stations are regarded as the cornerstone of electric vehicle (EV) development and utilization. Electric vehicle charging stations (EVCSs) are now energized via standalone microgrids that utilize renewable energy sources and reduce the stress on the utility grid. However, the control and energy management of EVCSs are challenging tasks because they are nonlinear and time-varying. This study suggests a fractional-order proportional integral (FOPI) controller to improve the performance and energy management of a standalone EVCS microgrid. The microgrid is supplied mainly by photovoltaic (PV) energy and utilizes a battery as an energy storage system (ESS). The FOPI's settings are best created utilizing the grey wolf optimization (GWO) method to attain the highest performance possible. The grey wolf is run for 100 iterations using 20 wolves. In addition, after 80 iterations for the specified goal function, the GWO algorithm almost discovers the ideal values. For changes in solar insolation, the performance of the proposed FOPI controller is compared with that of a traditional PI controller. The Matlab/Simulink platform models and simulates the EVCS's microgrid. The results demonstrate that the suggested FOPI controller significantly improves the transient responsiveness of the EVCS performance compared to the standard PI controller. Despite all PV insolation disruptions, the EV battery continues to charge while the ESS battery precisely stores and balances PV energy changes. The results support the suggested FOPI control's robustness to parameter mismatches. The microgrid's efficiency fluctuations with the insolation level and state of charge of the EV battery are discussed.

Keywords: fractional-order proportional integral (FOPI); electric vehicle charging station (EVCS); grey wolf optimization (GWO)

Citation: Zaid, S.A.; Bakeer, A.; Albalawi, H.; Alatwi, A.M.; AbdelMeguid, H.; Kassem, A.M. Optimal Fractional-Order Controller for the Voltage Stability of a DC Microgrid Feeding an Electric Vehicle Charging Station. *Fractal Fract.* **2023**, *7*, 677. https://doi.org/10.3390/fractalfract7090677

Academic Editors: Germán Ardúl Muñoz Hernández and Fermi Guerrero-Castellanos

Received: 8 August 2023
Revised: 25 August 2023
Accepted: 6 September 2023
Published: 9 September 2023

1. Introduction

Electric vehicles (EVs) are currently replacing conventional internal combustion engine (ICE) cars [1,2]. Actually, ICEs have several flaws that EVs can help overcome. Compared to ICEs, EVs produce little pollution, are more energy efficient, make less noise, and require less maintenance. The infrastructure of the charging stations, the duration of the charging process, and the impact of these stations on the current electrical grid are just a few of the challenges that have yet to be overcome. Rapid charging techniques may drastically decrease the charging time to a few minutes [3,4]. However, these methods place heavy electrical demands and negatively affect the electricity grid. Numerous issues would be created, such as severe overload, voltage fluctuation, and voltage instability, particularly when many charging stations are connected concurrently to the utility grid [5,6]. The improvement of the electrical system is one remedy for these issues, but it will be expensive. Utilizing an energy storage system (ESS) that may serve as a buffer between the utility and the EV charging station (EVCS) is another superior approach [7]. The utility grid will feel less strain with the deployment of an ESS, but there will still be difficulties due to the anticipated high number of EVCSs in the future.

If most of the grid electricity used at the charging stations comes from fossil fuels, the claim that electric vehicles are ecologically beneficial may not hold up. Therefore, it is necessary to use renewable energy sources in EVCSs to emphasize the effects of EVs on the environment. It is well known that renewable sources are typically intermittent rather than continuous. In order to resolve the discontinuity in these sources, ESSs are used.

Biogas, PV, and wind energy systems are the most often employed renewable energy sources for EV charging stations [8,9]. Compared to wind energy systems, PV energy systems are easier to use and more efficient. PV electricity is, therefore, more desirable for EV charging stations. PV-based charging stations have been the subject of several research articles [10]. The authors of one study put forth a concept for an EV charging station powered by solar energy [11]. Additionally, the authors provide a mathematical model of the charging station and employ simulation tools to evaluate the system's performance under varying conditions. The simulation findings demonstrate that the suggested charging station can operate independently of the power grid and satisfy an EV's charging needs. The authors of [12] suggest a creative method for developing an EV charging station that combines vehicle-to-grid (V2G) technology with solar and wind energy. The authors' detailed system design includes a solar panel array, a wind turbine, a battery energy storage system, an EV charging station, and a V2G interface. The technology is meant to charge EVs and feed extra electricity generated during high demand back into the grid. According to the scientists, the suggested system can deliver dependable and sustainable energy for grid support and EV charging. The authors of [13] propose a solar PV-powered EV charging station. To increase the efficiency of the charging process, the study discusses the design of a PV array, a DC–DC converter, and using a perturb and observe method. According to the simulation results, electric car charging at the station may be efficient and dependable. A control method that guarantees a charging station's steady functioning while optimizing the use of renewable energy sources is suggested by [14]. A secondary control loop optimizes the power flow between the various energy sources based on the available energy and the demand for EV charging. By contrast, a primary control loop smooths the voltage and current of the converter as part of the control strategy. Research on the viability of a hybrid system that combines solar and wind power to provide energy for a grid-connected EV charging station is presented in [15]. The research uses HOMER software (V4.9) to simulate the system, which optimizes the system's architecture by identifying the ideal mix of solar and wind resources, energy storage capability, and EV charging demand. According to the findings, the hybrid system is technically possible and has a respectable payback period. The report also analyzes the hybrid system's potential advantages, such as promoting local economic growth by generating green employment, lowering emissions, and strengthening energy security. In [16], a hybrid energy power system that uses the utility grid as a backup is utilized to charge EVs using the electric railway power system. Ref. [17] integrated PV electricity into an EV quick charging station using PV panels and a bank of batteries using a three-level boost converter. Although output capacitor voltage balancing must be considered, this relieves some pressure on switching devices.

Several renewable energy systems have used fractional-order control (FOC), a relatively novel control method [18]. FOC is a development of conventional integer-order control and has several benefits over traditional control methods, including higher performance, better resilience, and more flexibility. Despite these benefits, FOC has certain drawbacks as well. Its intricacy, difficulty of implementation, and computationally demanding nature are the key drawbacks. Ref. [19] presents a survey of recent advances in FOC autotuning techniques. A method for controlling fractional-order semilinear systems that have limitations given by linear equations was introduced by [20]. The suggested approach is used in a drug delivery system to regulate the drug concentration, and the results of extensive simulations are used to evaluate its performance. However, the technique has a complex procedure. Ref. [21] introduces a new adaptive FOPID compensator that self-adjusts fractional instructions to get the most power possible out of a standalone PV system as the environment changes. However, the numerical computations are very tedious.

This study presents an implementation of the FOPI controller to manage and control a photovoltaic-powered autonomous EV charging station. The ESS's battery is charged and discharged using a bidirectional converter, while the EV is charged using a unidirectional converter. The energy management and control of the proposed microgrid are based on optimal fractional-order controllers. The system's main objective is to maintain DC bus voltage regulation, control the storage battery charging, control the EV charging, and manage the system energy. The gains of the fractional-order controller are optimally chosen based on the GWO optimization technique. Moreover, performance comparisons were carried out between the proposed FOPI controller and the traditional PI controller. The proposed EVCS microgrid was modeled and simulated using the Matlab/Simulink platform. The following are this study's objectives:

- To enhance the functionality of the suggested EV charging station, FOPI controllers were incorporated.
- The suggested FOPI controller's ideal gains were determined using the metaheuristic optimization technique GWO.
- The suggested system's performance using the FOPI controller and the traditional PI were compared. The performance of the controller was evaluated under various solar isolation disturbances.
- Modeling the suggested system using Matlab. In order to determine the impact of fluctuations of the solar insolation on the microgrid's response, the system's performance was evaluated.
- The suggested control system's durability was explored in the face of parameter uncertainty.

This paper is organized as follows: the suggested charging station is shown in Section 2; Section 3 describes the microgrid modeling and design considerations of the charging station; the proposed control structure is presented in Section 4; the outcomes of the simulation are covered in Section 5; and, finally, the conclusions are presented in Section 6.

2. The Studied EVCS Description

Figure 1 depicts the proposed EVCS system's design. The off-grid EVCS system uses solar energy as its source of electricity. It is connected to a PV array, producing EVCS electricity. The primary energy source for the EVCS is the PV panel. However, the generated energy varies depending on various environmental factors, like the amount of solar insolation. Therefore, ESS batteries are typically utilized to address the issue of intermittent energy supply. A boost converter is attached to the PV's output terminals. Its purpose is to use the PV panel's maximum power point tracking (MPPT) condition by matching the PV voltage level to that of the DC link. The energy storage and EV charging converters are connected to the DC bus. Typically, these converters are DC/DC converters. A unidirectional buck converter is used to manage the charging process of the EV battery. The energy storage converter, on the other hand, is a bidirectional DC/DC converter. Its function is to regulate how the storage battery is charged and discharged. Additionally, it plays a role in controlling the DC bus voltage to counteract changes in EV load and insolation level. The following paragraphs will discuss the modeling and operating principles of these converters.

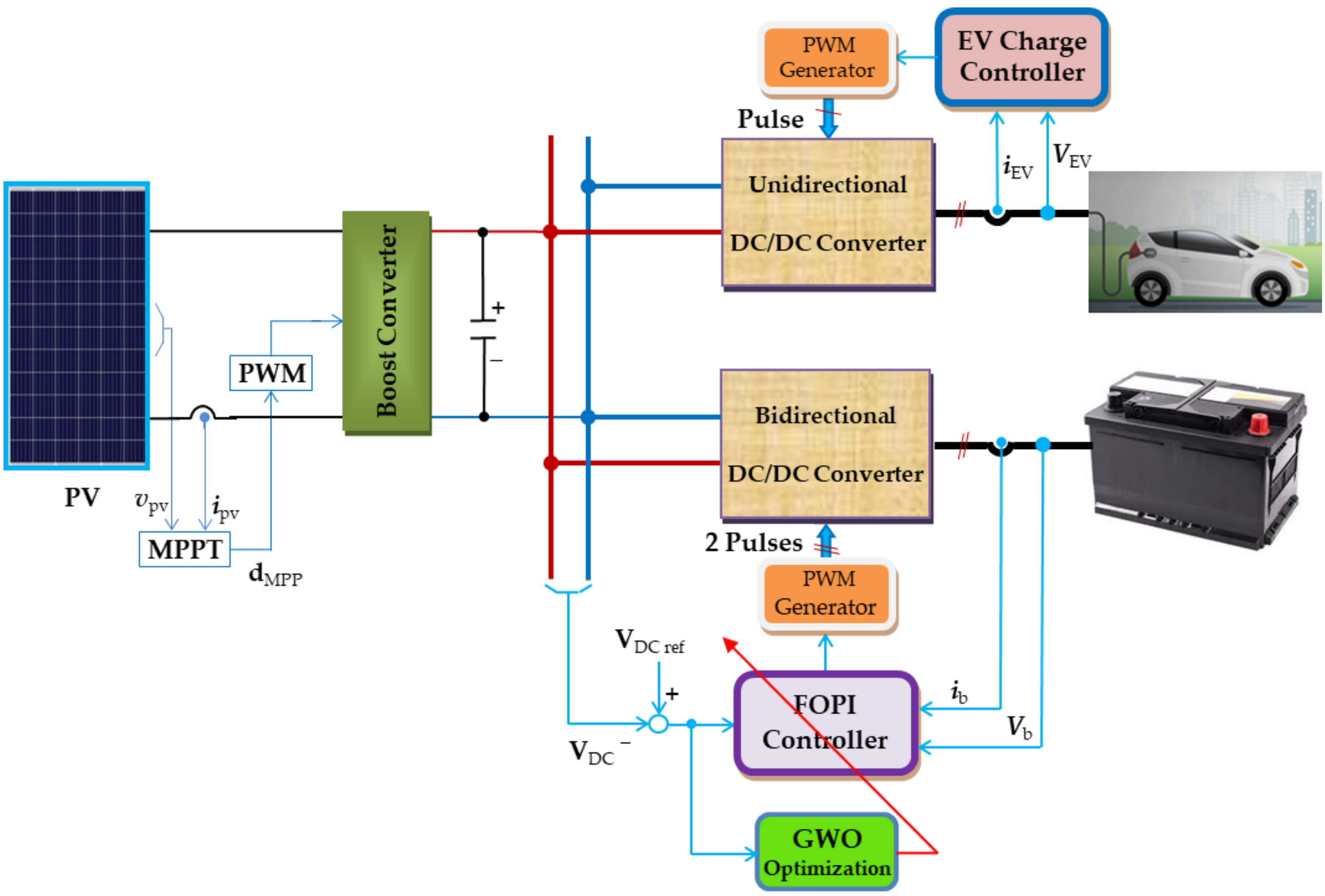

Figure 1. The proposed microgrid of the charging station.

3. Modeling of the EVCS Microgrid

For the purpose of designing the control system of the proposed EVCS microgrid, the microgrid model must be identified carefully. Hence, the model of the EVCS microgrid will be discussed in the following subsections. Specifically, the model of the power, energy, and DC/DC converters will be explained. The PV array model is common in the literature, so it will not be repeated here.

3.1. Power and Energy Model

The energy and power relationships of the EVCS microgrid are presented in this section. It is assumed that the EV station (P_{EV}) is constant and instantaneous PV-panel power (P_{pv}) is given by [11]:

$$P_{pv} = \begin{cases} P_{max}\left(1 - \frac{t^2}{36}\right) & -6 \le t \le 6 \\ 0 & 6 \le t \le 18 \end{cases} \quad (1)$$

where (t) is the time in hours starting at noon and (P_{max}) is the maximum power generated by the PV. It is assumed that the origin of the time axis is fixed at noon when insolation is at its highest. It is believed that solar energy lasts for 12 h, beginning at 6:00 a.m.

The instantaneous power of the proposed microgrid is governed by:

$$P_{EV} = P_{pv} - P_b - P_{loss} \quad (2)$$

where (P_{loss}) is the microgrid power loss and (P_b) is the ESS battery power. A useful equation for the design purpose is given by:

$$P_{max} = 3P_{EV} - \frac{\int_0^T P_{loss} dt}{T} \tag{3}$$

where (T) is the time period. The state of charge (SOC_b) of the ESS battery may be determined using:

$$SOC_b = \frac{\int P_b dt}{E_{rated}} \tag{4}$$

where (E_{rated}) is the ESS battery's rated energy.

The ESS battery has a maximum stored energy ($\Delta E_b|_{max}$) determined using [11]:

$$\Delta E_b|_{max} = 12.53 P_{EV} - 2\int_0^T P_{loss} dt \tag{5}$$

3.2. EVCS Converter Model

There are two charging converters in the suggested system. A straightforward unidirectional buck converter serves as the EV charging converter. The energy storage battery, however, is a bidirectional DC/DC converter. Figure 2 displays the circuit diagram for the converters, where $L_1 = L_2 = L$. The unidirectional converter is included in the operation, modeling, and analysis of the bidirectional converter. Continuous mode is necessary for the converter's operation. The converter was made of a filter, two antiparallel diodes, and two transistors (Q_1, Q_2). The storage battery and the DC bus are connected to the converter terminals. (E_b, r_b) denote the internal voltage and resistance of the ESS battery. The filter inductance is believed to be sufficiently large to retain enough energy to charge/discharge the ESS battery. Therefore, the continuous conduction mode of operation is ensured. Buck mode and boost mode are the converter's two operating modes. The bidirectional converter is used to discharge the battery while switch Q_1 acts as a diode and switch Q_2 is in boost mode. However, it works in the buck mode, the battery charging mode, when switch Q_1 is turned on and switch Q_2 functions as a diode. The state-space model of the converter is given as follows:

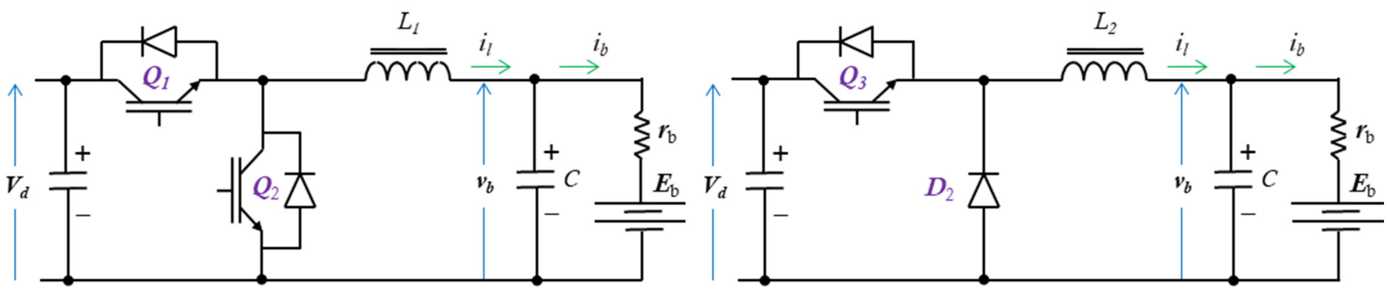

Figure 2. The circuit diagram of the (**a**) bidirectional converter and (**b**) unidirectional converter.

Charging mode:

$$\dot{x} = Ax + Bu_1 + D_1 \tag{6}$$

$$x = \begin{bmatrix} v_c \\ i_l \end{bmatrix},\ A = \begin{bmatrix} \frac{1}{C} & \frac{-1}{Cr_b} \\ 0 & \frac{-1}{L} \end{bmatrix},\ B = \begin{bmatrix} 0 \\ \frac{V_d}{L} \end{bmatrix},\ u_1 = \begin{cases} 1 & Q_1\ is\ on \\ 0 & Q_1\ is\ off \end{cases},\ D_1 = \begin{bmatrix} \frac{E_b}{Cr_b} \\ 0 \end{bmatrix} \tag{7}$$

where (L, C) are the filter's inductance and capacitance, (i_l, v_c) are the inductor's current and capacitor's voltage, and the DC link voltage is (V_d).

Discharging mode:

$$\dot{x} = Ax - Bu_2 + D_2 \tag{8}$$

$$u_2 = \begin{cases} 1 & Q_2 \text{ is on} \\ 0 & Q_2 \text{ is off} \end{cases}, \quad D_2 = \begin{bmatrix} \frac{E_b}{Cr_b} \\ \\ \frac{V_{dc}}{L} \end{bmatrix} \tag{9}$$

4. Proposed Control Structure

The three controllers responsible for the stable operation of the proposed microgrid, as depicted in Figure 3, include the MPPT controller, the EV converter controller, and the DC link regulator using the DC–DC converter of the battery energy storage. The primary task of the MPPT regulator is to continually capture the maximum power output from the photovoltaic (PV) array. It achieves this by calculating and providing the appropriate duty cycle to the boost converter, ensuring the MPPT is effectively maintained. On the other hand, the EV converter controller plays a crucial role in ensuring a well-regulated charging process for the electric vehicle. Additionally, the converter's controller of the battery energy storage regulates both the DC bus voltage and the charge/discharge operations of the energy storage system (ESS). It comprises two loops: the first loop (i.e., outer loop) controls the DC bus voltage, while the second (i.e., inner loop) regulates the battery current. In this section, we will not delve into the details of the MPPT algorithm, as it is a relatively simple approach based on the perturb and observe (P&O) technique. However, maintaining the DC link voltage stable across the terminals of the EV charger is paramount for ensuring the electric vehicle's smooth functioning during the charging process. It is crucial to understand that the EV acts as a power-consuming load, and it relies on either the photovoltaic (PV) system or the battery to provide the necessary power, based on their availability.

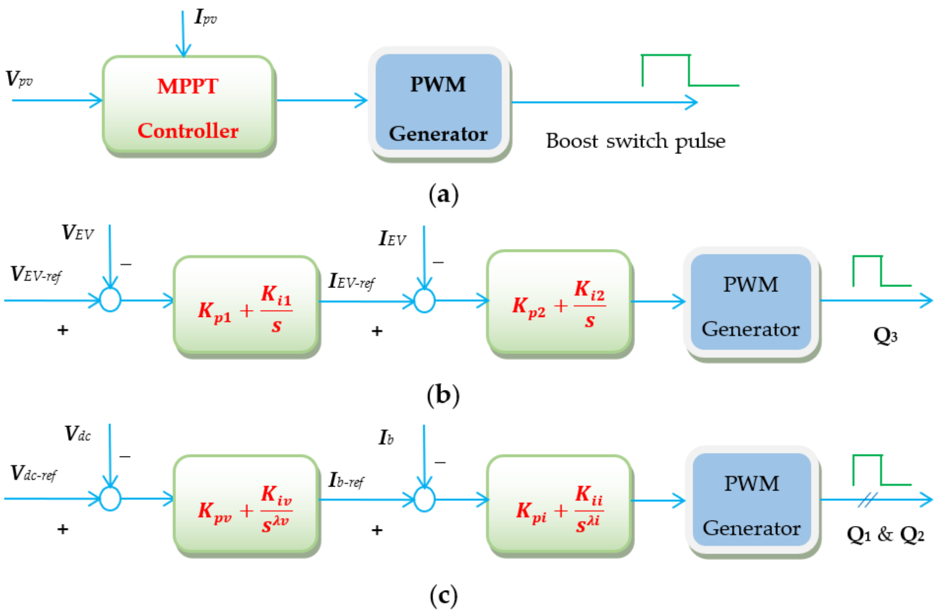

Figure 3. Structure of each control stage for the proposed standalone EV charging station: (**a**) MPPT regulator, (**b**) EV converter controller, and (**c**) DC bus based on the BESS converter.

4.1. Proposed Fractional-Order Controller

The objective of this regulator is to maintain a steady DC link voltage (V_{dc}) at a specific set value ($V_{d\text{-}ref}$). To achieve this, the controller adjusts the charging and discharging processes of the battery energy storage accordingly. The proposed controller is constructed using the fractional-order proportional integral (FOPI), which is employed to design both the inner loop, which maintains the DC link stability, and the outer loop, which regulates the battery current.

The utilization of fractional operators in the controller enables the representation of any real number through a sophisticated and versatile integral or differential notation [22]. The fundamental mathematical correlation between the FO differential and integral operator, for a certain order q, can be expressed in the following function:

$$D^{q}_{lb,ub}f(t) = \begin{cases} \frac{d^q}{dt^q} f(t) & q > 0 \\ f(t) & q = 0 \\ \int_{lb}^{ub} f(t) d\tau^{-q} & q < 0 \end{cases} \tag{10}$$

where l_b denotes the lower band and u_b denotes the upper band; when the value of the order q is positive (that is, q > 0), it is classified as a FO differential transfer function; conversely, when the value of the order q is negative (that is, q < 0), it is classified as a first-order integral.

Scholars have proposed various definitions in order to make the concept of fractional order (FO) more accessible, as it can be challenging to comprehend its physical implications. One such definition, known as the Riemann–Liouville (R-L) approach, offers a method to calculate the function's order derivative, aiding our understanding of the underlying principles of FO [23]:

$$D^{q}_{lb,ub}f(t) = \frac{1}{\Gamma(n-q)}\left(\frac{d}{dt}\right)^{n} \int_{lb}^{ub} \frac{f(\tau)}{(t-\tau)^{q-n+1}} d\tau \tag{11}$$

where $n \in$ N, n − 1 < q < n, and the Gamma function $\Gamma(w)$ is defined as,

$$\Gamma(w) = \int_0^{\infty} t^{w-1} e^{-t} dt \tag{12}$$

Equation (11)'s fractional derivative of R-L may be transformed using the Laplace method to provide Equation (13)'s answer [22]. Caputo's definition, a second definition related to the concept of FO, is used to express the time domain representation of the q order of the function *f(t)*, as in Equation (14) [24].

$$\mathcal{L}\left\{D_0^q f(t)\right\} = s^q F(s) - \sum_{z=0}^{n-1} s^z \left(D_0^{q-z-1} f(t)\right)\Big|_{t=0} \tag{13}$$

$$D^{q}_{lb,ub}f(t) = \begin{cases} \frac{1}{\Gamma(n-q)}\left(\int_{lb}^{ub} \frac{f^n(\tau)}{(t-\tau)^{1-n+q}} d\tau\right) & n-1 < q < n \\ \left(\frac{d}{dt}\right)^n f(t) & q = n \end{cases} \tag{14}$$

When the Laplace transformation is applied to (14), the integral order of the equation is accompanied by an initial condition. This initial condition holds significant physical meaning and can be explained through Equation (15), where s is the Laplace operator.

$$\mathcal{L}\left\{D_0^q f(t)\right\} = s^q F(s) - \sum_{z=0}^{n-1} s^{q-z-1} f^{(z)}(0) \tag{15}$$

Using the FO operators in the time domain involves performing complicated math calculations. To implement FO operators, we often use the recursive approximation method [25,26]. The Laplace transformation of the qth derivative is a way to represent it using a different mathematical formula, as follows:

$$s^q \approx K \prod_{k=-N}^{N} \frac{s+\omega'_k}{s+\omega_k} \tag{16}$$

where

$$K = \omega_h^q,$$
$$\omega_k' = \omega_b \left(\frac{\omega_h}{\omega_b}\right)^{\frac{k+N+(1-q)/2}{2N+1}},$$
$$\omega_k = \omega_b \left(\frac{\omega_h}{\omega_b}\right)^{\frac{k+N+(1+q)/2}{2N+1}},$$

and (N) is the approximation order of the Oustaloup method in the effective frequency range $[\omega_b, \omega_h]$ that can be chosen as $[-1000, 1000]$ rad/s. In the present study, we chose a value of N equivalent to 5.

The present study utilizes the FO proportional integral controller consisting of three tuning parameters: proportional gain (K_p), integral gain (K_i), and integral fractional order λ. Controllers constructed with these particular parameters have been discovered to exhibit enhanced stability, transient time, and overall precision in comparison to conventional PI regulators [27]. Furthermore, this controller offers greater adaptability and robustness in the face of system disruptions, enabling it to manage various disturbances effectively. Moreover, Equation (17) presents the comprehensive expression for the transfer function of the FOPI in Laplace form, denoted as $G_c(s)$, where λ is frequently in the range of [0, 1]. At the same time, Figure 4 illustrates the basic configuration of the control structure.

$$G_c(s) = K_p + K_i\left(\frac{1}{s}\right)^{\lambda} \tag{17}$$

The voltage across the DC link is monitored and compared to a set reference voltage. The FOPI controller is responsible for regulating the voltage difference by producing the desired battery current reference value. This reference value helps ensure proper control and management of the DC link voltage. Hence, the desired ESS's battery current, as determined by the reference, is then compared to the actual battery current. The FOPI controller utilizes this comparison to compute and modify the duty cycle of the bidirectional DC/DC converter. The dual loop control system ensures that the current drawn from the battery remains at a safe level, thus providing protection.

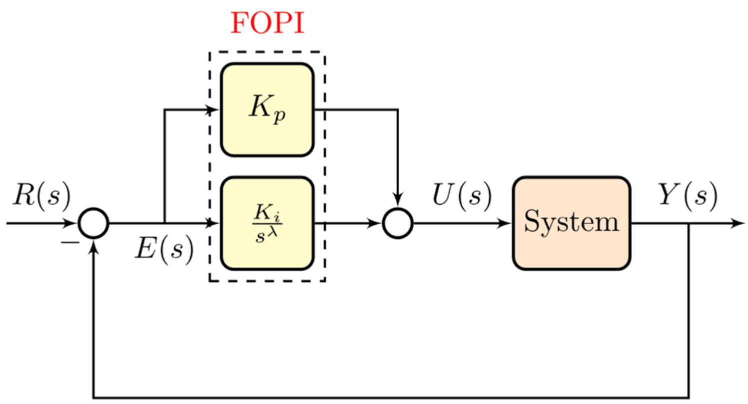

Figure 4. The FOPI controller's fundamental architecture.

4.2. Utilized Optimization Approach

Determining the FOPI parameters by trial and error can be complex, relying greatly on the practitioner's skill and knowledge. It can be quite a daunting challenge to identify suitable values for the proposed FOPI parameters. However, it is of utmost importance to carefully carry out this process to enhance the system's performance and ensure its stability, preventing disruptions. To achieve this, a metaheuristic optimization technique, GWO, is employed to identify the most optimal values for the FOPI controller's parameters.

Recently, there has been a surge in the popularity of a particular optimization technique that draws inspiration from the behaviors exhibited by gray wolves. This technique, known as gray wolf optimization (GWO), is highly regarded as a meta-heuristic approach [28]. In a wolf pack, a well-defined social structure based on dominance exists. These packs typically consist of members ranging from 5 to 12 individuals. Leading this pack is the alpha wolf (α), who holds the highest position of authority. Assisting the alpha is the beta wolf (β), a trusted ally who aids in making important decisions for the group. On the other end of the hierarchy, we find the omega wolf (ω) occupying the lowest rank. This wolf serves as a scapegoat and is often subjected to the blame for any mishaps or conflicts within the pack. The remaining wolves in the group are known as delta wolves (δ), and they dutifully follow the leadership of the alphas and betas, embodying a sense of loyalty and obedience. The GWO method involves several roles, as depicted in Figure 5. To successfully capture prey, the method consists of three primary steps: firstly, the wolves engage in a search to locate the prey and closely approach it; secondly, they encircle the prey, restricting its movement; and finally, they initiate an attack to capture and ultimately bring down the prey.

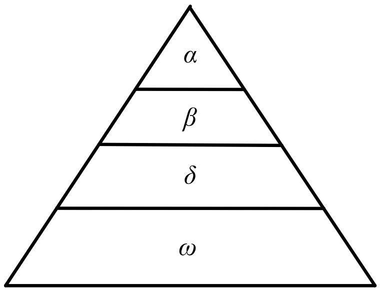

Figure 5. The general hierarchy structure of the grey wolves.

The environment in which the prey exists can be represented using Equation (18), where $\vec{P}_{pi}$ is the position of the prey, $\vec{P}_i$ is the position of the grey wolf, $\vec{S}$ is the distance between them, $\vec{A}$ and $\vec{C}$ are vectors computed from Equations (20) and (21), respectively.

$$\vec{S} = \left| \vec{C}\vec{P}_{pi} - \vec{P}_i \right| \tag{18}$$

$$\vec{P}_{i+1} = \vec{P}_{pi} - \vec{A}\vec{S} \tag{19}$$

$$\vec{A} = 2\vec{a}\ \vec{n}_1 - \vec{a} \tag{20}$$

$$\vec{C} = 2\vec{n}_2 \tag{21}$$

where

$$\vec{a} = 2 - \frac{2t}{Max\_iter} \tag{22}$$

where $\vec{n}_1$ and $\vec{n}_2$ are random numbers in the range of zero to one. The value of the factor $\vec{a}$ gradually decreases from two to zero as the number of iterations increases. The divergence technique is employed when looking for a prey location with $|A| > 1$, whereas the convergence technique is utilized to obtain prey in locations with $|A| < 1$. The hunting process involves the utilization of α, then β, and δ as presented in Equations (23) to (25).

$$\begin{cases} \vec{S}_\alpha = \left| \vec{C}_1\vec{P}_{\alpha i} - \vec{P}_i \right| \\ \vec{S}_\beta = \left| \vec{C}_2\vec{P}_{\beta i} - \vec{P}_i \right| \\ \vec{S}_\delta = \left| \vec{C}_3\vec{P}_{\delta i} - \vec{P}_i \right| \end{cases} \tag{23}$$

$$\begin{cases} \vec{P}_1 = \vec{P}_{\alpha i} - \vec{A}_1 \vec{S}_\alpha \\ \vec{P}_2 = \vec{P}_{\beta i} - \vec{A}_2 \vec{S}_\beta \\ \vec{P}_3 = \vec{P}_{\delta i} - \vec{A}_3 \vec{S}_\delta \end{cases} \tag{24}$$

$$\vec{P}_{i+1} = \frac{1}{3}\left(\vec{P}_1 + \vec{P}_2 + \vec{P}_3\right) \tag{25}$$

4.3. Objective Function Definition

The tuning process of the FOPI gains for the dual loop of the BESS controller is presented in Figure 6a. The following points summarize the GWO routine to find the optimal parameters of the proposed FOPI:

- Initialize the population of wolves, which are considered the candidate solutions for the FOPI parameters (i.e., six values).
- Simulate the proposed EVCS using the parameters generated from GWO.
- Calculate the objective function based on the integral square error (ISE) to quantify the control system's performance.
- Identify the population's alpha, beta, and delta wolves based on their fitness values. Alpha represents the best solution, beta the second-best, and delta the third-best.
- Update the positions of the remaining wolves in the population.
- Check the new updated positions of the grey wolves that remain within the constraints.
- Repeat the process until the termination criteria are achieved.

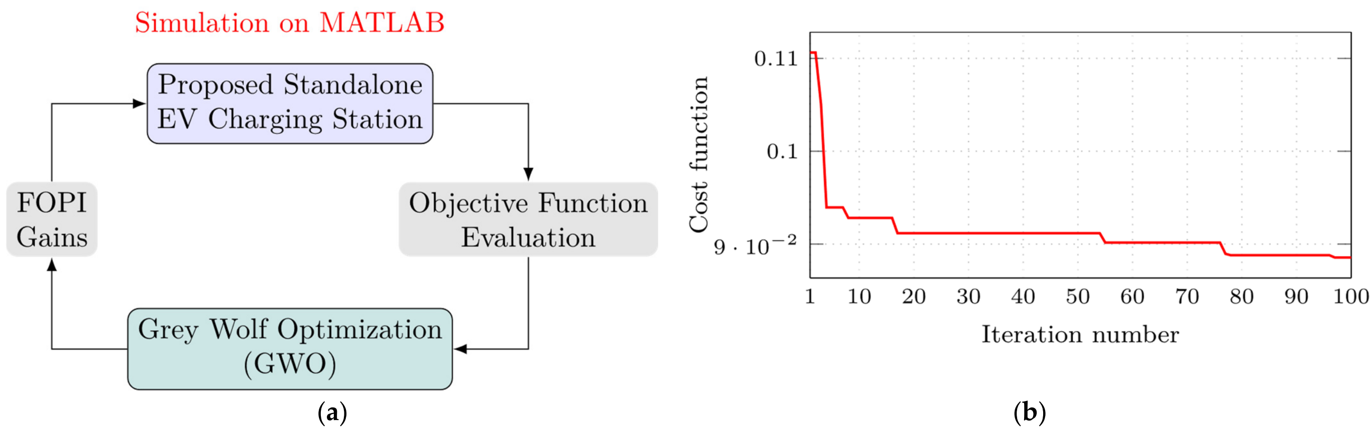

Figure 6. (**a**) The tuning procedure of the proposed FOPI gains to stabilize the EV charging station; (**b**) the convergence curve of the employed GWO to tune the FOPI gains.

Table 1 summarizes the associated parameters of the GWO. In Equation (26), the integral square error (ISE) is used as the fitness function for the GWO, in which t_{sim} is the simulation time. The GWO algorithm was executed on a personal computer with an Intel CoreTM i5-8265U CPU running at 1.60 GHz and 16 GB of RAM. The applied GWO's convergence curve is shown in Figure 6b, and Table 2 lists the best FOPI values. The GWO algorithm that has been proposed successfully attains a remarkably low fitness function value of around 0.0886. Furthermore, it is worth mentioning that the GWO algorithm can approach the optimal parameters in a relatively short period, typically within 80 iterations, when considering the *ISE* objective function.

$$ISE = \int_0^{tsim} \left(V_{dc-ref} - V_{dc}\right)^2 dt \tag{26}$$

Table 1. Parameters of the GWO for tuning the gains of the proposed FOPI.

Description	Value
Number of wolves	20
Number of iterations	100
Minimum range	[0,0,0,0,0,0]
Maximum range	[50,500,1,10,50,1]

Table 2. The optimal parameters of the FOPI using GWO.

Control Loop	Parameter	Value
Inner loop (DC link voltage stabilization)	K_{pv}	8.809
	K_{iv}	341.984
	λ_v	0.753
Outer loop (BESS current regulation)	K_{pi}	3.797
	K_{ii}	48.138
	λ_i	0.874

5. Simulation Results and Discussion

The suggested EVCS's microgrid, represented in Figure 3, is simulated using the Matlab/Simulink platform to validate the paper's hypothesis. The microgrid's parameters are listed in Table 3, including the PV array, ESS battery, EV battery, and converters. The converters' switching frequency utilized for the PWM carrier is 4 kHz.

Table 3. The parameters of the EVCS's microgrid.

Item	Item	Value
EV Battery	I_n, V_n	6.5 Ah, 3.7 V
	I_{ch}	3 A
	I_{disch}	5 A
ESS Battery	I_n, V_n	65 Ah, 12 V
	I_{ch}	13 A
PV Array (Copex-P120)	Type	Polycrystalline
	MPPT	120 W
	V_{oc}	19.2 V
	I_{sc}	8.82 A
Filter	C	1000 µF
	C_{dc}	2200 µF
	L	560 µH

Figure 7 displays the DC link voltage performances for FOPI and traditional PI controllers in response to step changes in solar irradiation. It may be seen in Figure 7a that the DC bus voltage closely follows its reference value precisely for both controllers. There is no steady-state error for both the FOPI and traditional PI controller responses. Nevertheless, the FOPI controller response has the lowest overshoot ($\leq$3.2%). On the other hand, the traditional PI controller response has an overshoot of $\leq$10.4%. Hence, the reduction in the system overshoot is (~1/3). Also, the settling time of the step response of DC link voltage using the FOPI controller has a lower value of $\leq$0.04 s. However, the settling time with the traditional PI controller is $\leq$ 0.1 s. Hence, the DC link voltage settling time reduction is (~2/5). These issues indicate a great improvement in the system response using the proposed FOPI controller. It is also noted that the DC link voltage response with the traditional PI controller has contaminated ripples that are not present in the response with the FOPI controller. The disturbance of solar radiation is presented in Figure 7b.

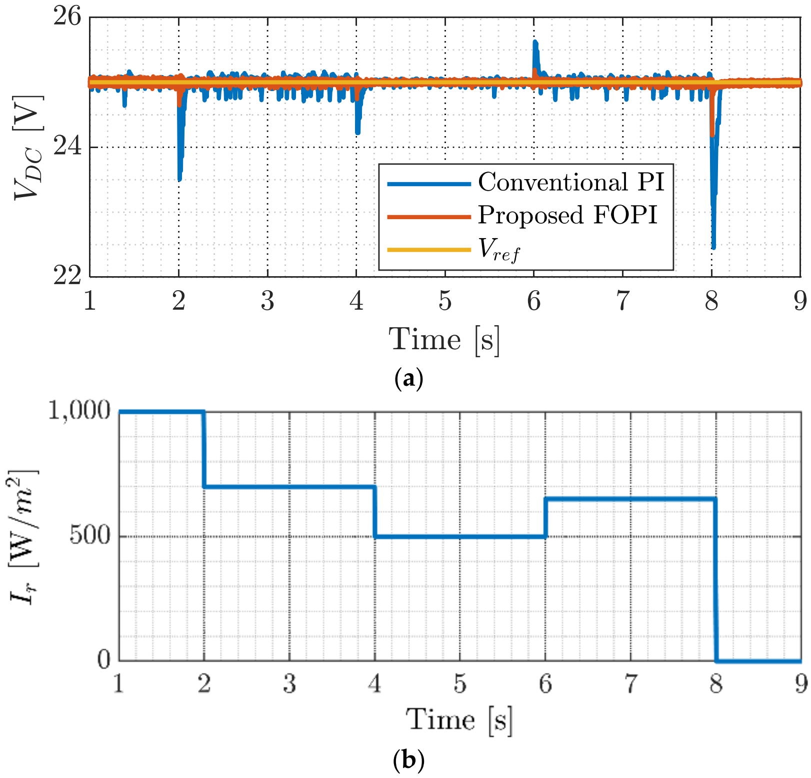

Figure 7. (**a**) Comparison of the DC bus voltage for both controllers under the variation of (**b**) PV insolation.

For the same disturbance profile in solar radiation, the charging station response with the proposed FOPI controller compared to the conventional PI controller is presented in Figure 8. The responses of the PV current corresponding to the step change in the solar radiation for both controllers are shown in Figure 8a,b. The PV current values match the MPPT circumstances. Figure 8c,d present the response of the PV voltage for both controllers. During the period [8 s to 9 s], the solar insolation drops to zero; therefore, the PV output voltage and current are zero. Figure 8e,f display the ESS battery's current response for both controllers. For both controllers, it tracks its reference fairly well. The DC bus voltage controller produces the reference value for the ESS battery's current. The charging and discharging procedures also keep track of their references and account for the radiation changes. Figure 8g,h display the ESS battery's voltage for the proposed FOPI and traditional PI controllers. When charged, its voltage rises, and when discharged, it falls. The performance of the ESS battery's SOC for the proposed FOPI and traditional PI controllers is shown in Figure 8i,j. The response of the SOC is nearly identical for both controllers. However, the charging and discharging processes are indicated. The insolation is about 70% for the first four seconds. Therefore, The EV battery may be charged, and the reserve may be stored in the ESS battery using the generated PV power. However, the insolation during the next two seconds, [4s to 6s], is just 50%, insufficient to provide the EV with energy. In order to make up for the decrease in solar energy, the storage battery drains. The insolation is 65% in the subsequent interval [6s to 8s], barely sufficient to charge the EV battery and keep the reserve in the ESS battery. Consequently, the SOC has a modest and positive slope. The sun insolation finally disappears during the period [8s to 9s]. As a result, no energy is created, and the ESS battery empties to make up for the solar energy.

Figure 9 shows the EV charging response with the proposed FOPI controller compared to the conventional PI controller. For both controllers in Figure 9a,b, the current of the EV closely matches its reference produced by the EV's converter controller. However, its response with the suggested FOPI controller is the best and has no overshoots or ripples. The voltage of the EV battery is shown in Figure 9c,d for both controllers. The replies remain the same as the EV battery charges continually. Figure 9e,f display the SOC of the EV battery for the two controllers, respectively. The responses remain the same as the EV battery charges continuously.

Figure 10 compares the proposed FOPI controller to the conventional PI controller for PV, ESS, and EV battery power. Both controllers' replies and how they track the PV's MPPT level remain constant. Figure 10a,b display the PV power responses, respectively. The irradiation in the first four seconds is around 70%. As a result, the PV energy produced is sufficient to charge the EV battery and store the remaining energy in the ESS battery. The following two seconds' insolation, from [4 s to 6 s], is 50%, insufficient to power the EV. In the ensuing period [6 s to 8 s], the insolation is 65%, barely sufficient to charge the EV battery and maintain the reserve in the ESS battery.

The sun's insolation completely fades between [8 s and 9 s]. As a result, no energy is produced, and to make up for the decrease in solar output, the ESS battery discharges. As seen in Figure 10c,d, the ESS battery drains to make up for the decrease in solar energy. Also, the procedures of charging/discharging account for the radiation changes. Figure 10e,f, which depict the two controllers, illustrate that the EV power is consistent under all circumstances. However, the proposed FOPI controller has a better response, free of disturbances and overshoots.

Table 4 summarizes the comparison of the maximum overshoot during each interval of the results using the proposed FOPI and the conventional PI controller.

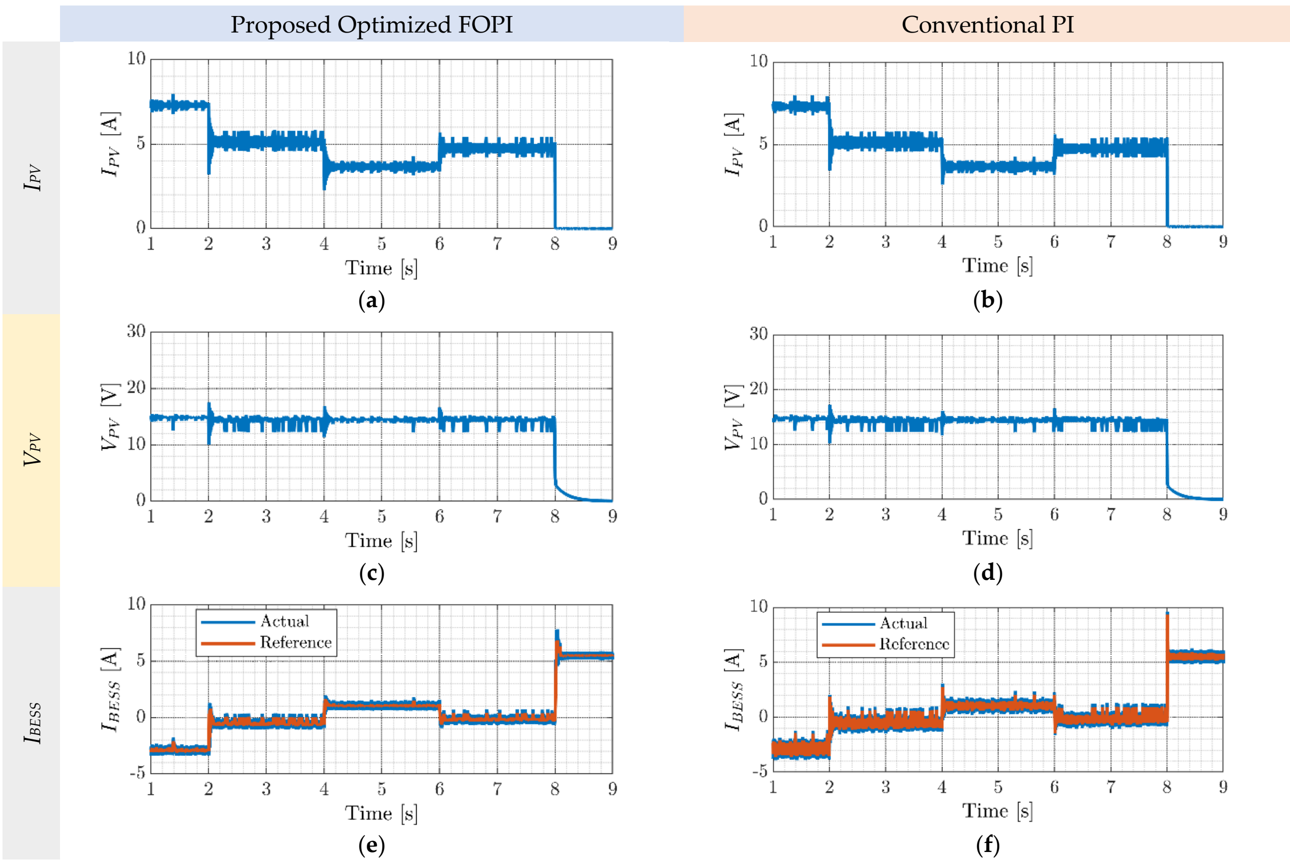

Figure 8. *Cont.*

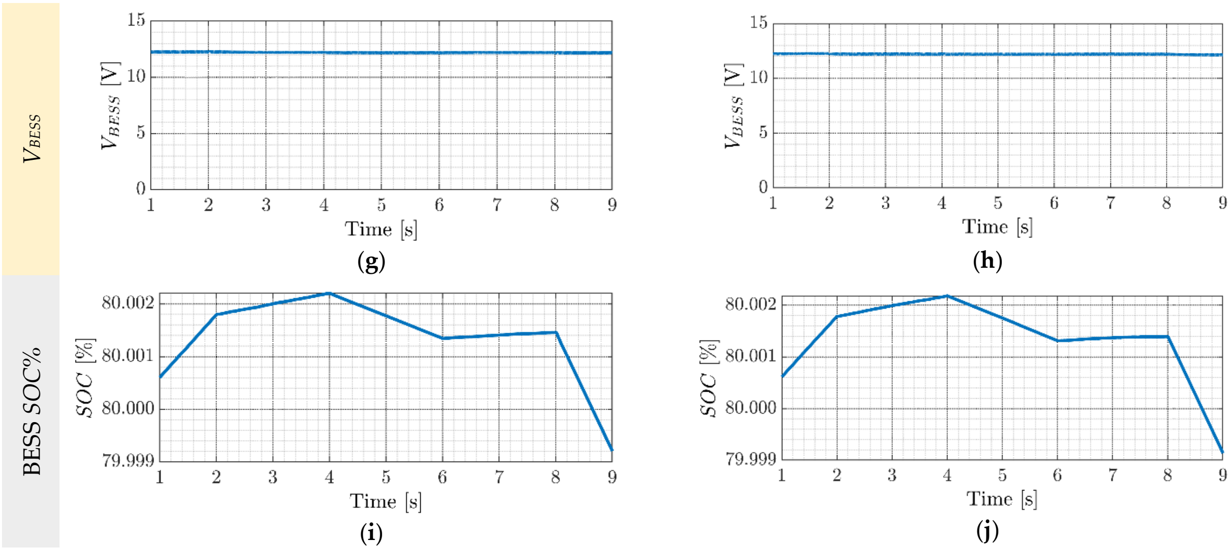

Figure 8. The charging station response with the proposed FOPI controller (**a**,**c**,**e**,**g**,**i**) compared to the conventional PI controller (**b**,**d**,**f**,**h**,**j**).

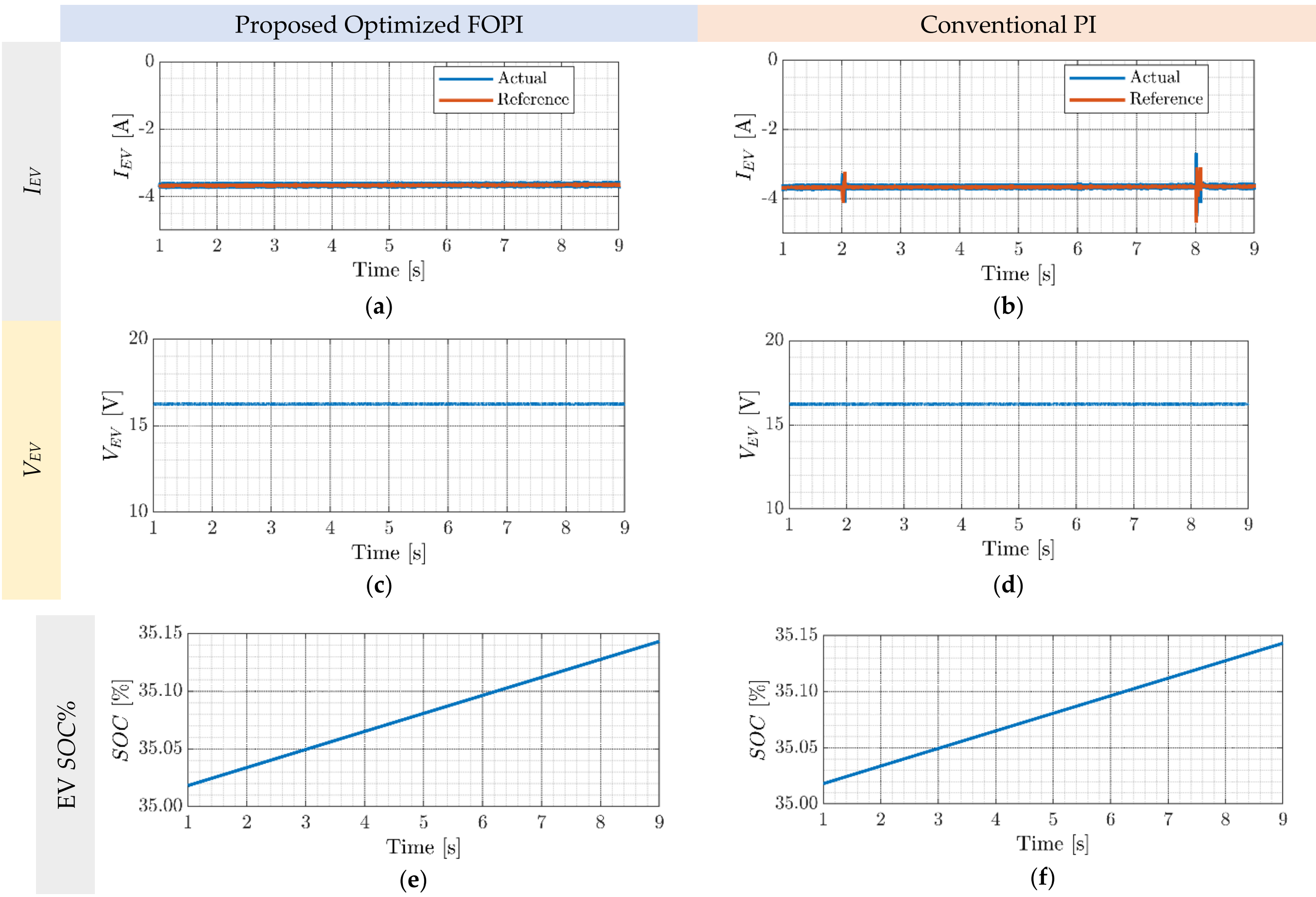

Figure 9. The EV charging response with the proposed FOPI controller (**a**,**c**,**e**) compared to the conventional PI controller (**b**,**d**,**f**).

Table 4. Maximum overshoot of the DC link voltage with the proposed FOPI and the conventional PI controller.

Time Interval (s)	Solar Irradiation Level (%)	Proposed FOPI	Conventional PI
1–2	100	1.6%	6%
2–4	70	1.2%	3.2%
4–6	50	0.8%	2.4%
6–8	65	3.2%	10.4%
8–9	0	0	0

Figure 11 depicts the FOPI controller's system efficiency fluctuation with insolation level and EV battery SOC. It should be noticed that both controllers' values for system efficiency are the same. As the EV_{SOC} increases, the system efficiency increases. However, that makes sense given that as the EV_{SOC} increases, the charging current decreases, the power losses decrease, and the EV's power decreases. Nevertheless, the power losses vary with the square of the current, but the EV's power is proportional to the current. Hence, microgrid efficiency increases. On the other hand, the efficiency decreases as the solar insolation level increases. That happened due to increased losses while charging the ESS battery of the EVCS's microgrid.

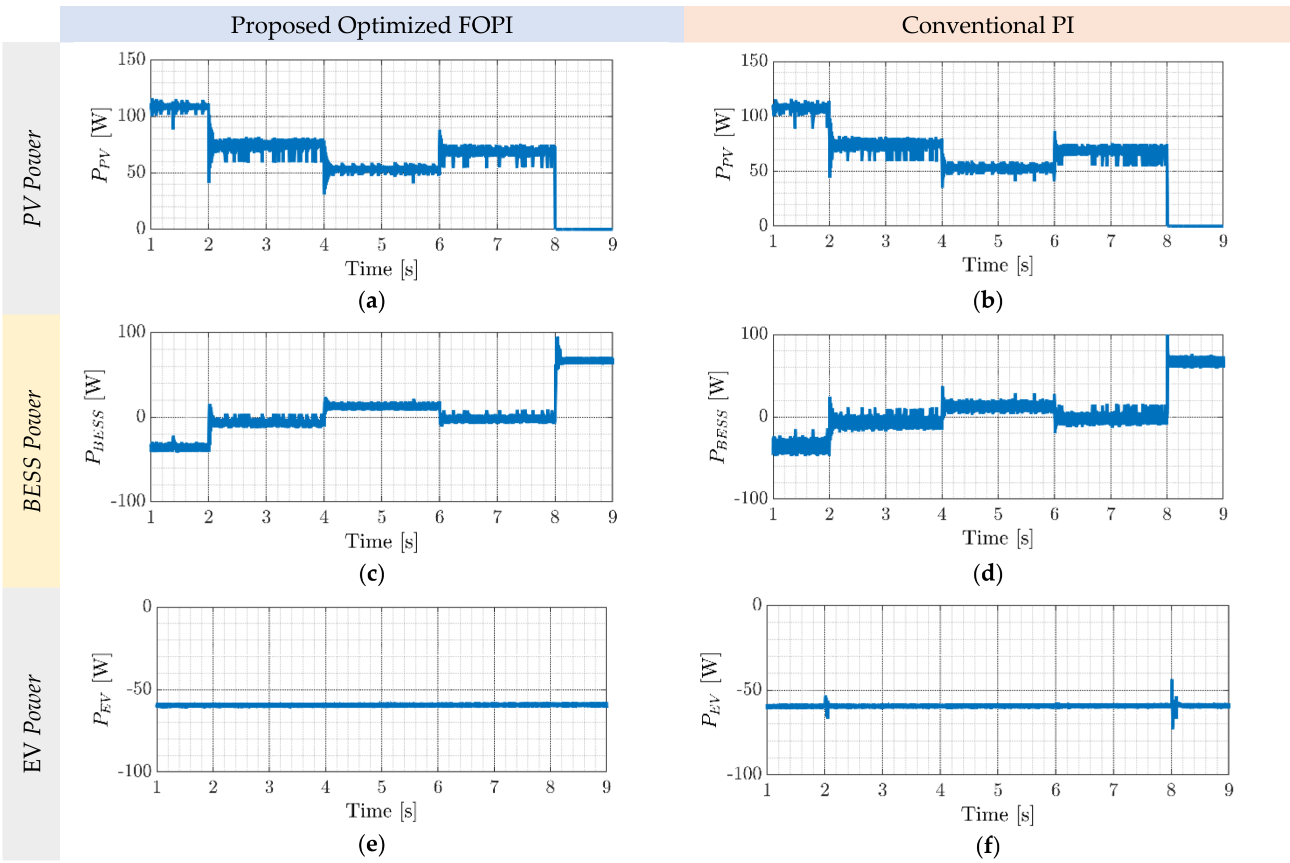

Figure 10. The power response of the charging station with the proposed FOPI controller (**a**,**c**,**e**) compared to the conventional PI controller (**b**,**d**,**f**).

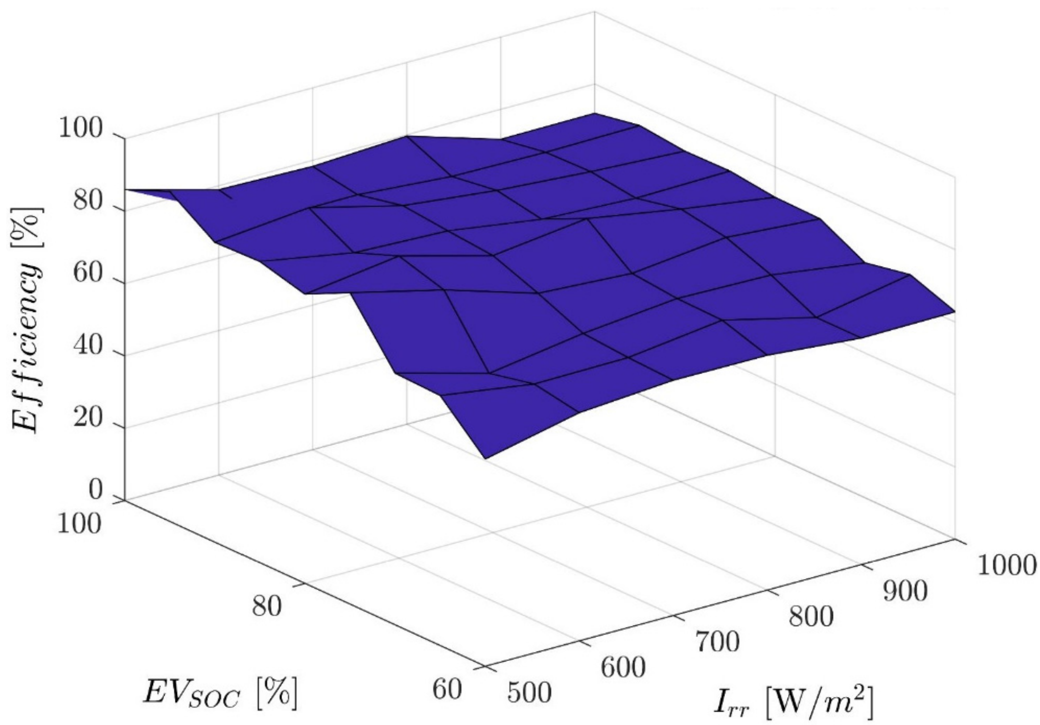

Figure 11. The system efficiency variations against the PV insolation and the EV battery SOC.

The impact of a ±10% variation in the value of the filter inductors (L_1, L_2) on the performance of the DC link voltage with the suggested controller is shown in Figure 12 to test the resilience of the proposed FOPI controller under parameter mismatches. It should be mentioned that the controller tracks the reference signal effectively. This demonstrates the control system's resistance to parameter mismatches. On the other hand, the overshoots are somewhat decreased, but the ripples are slightly enhanced.

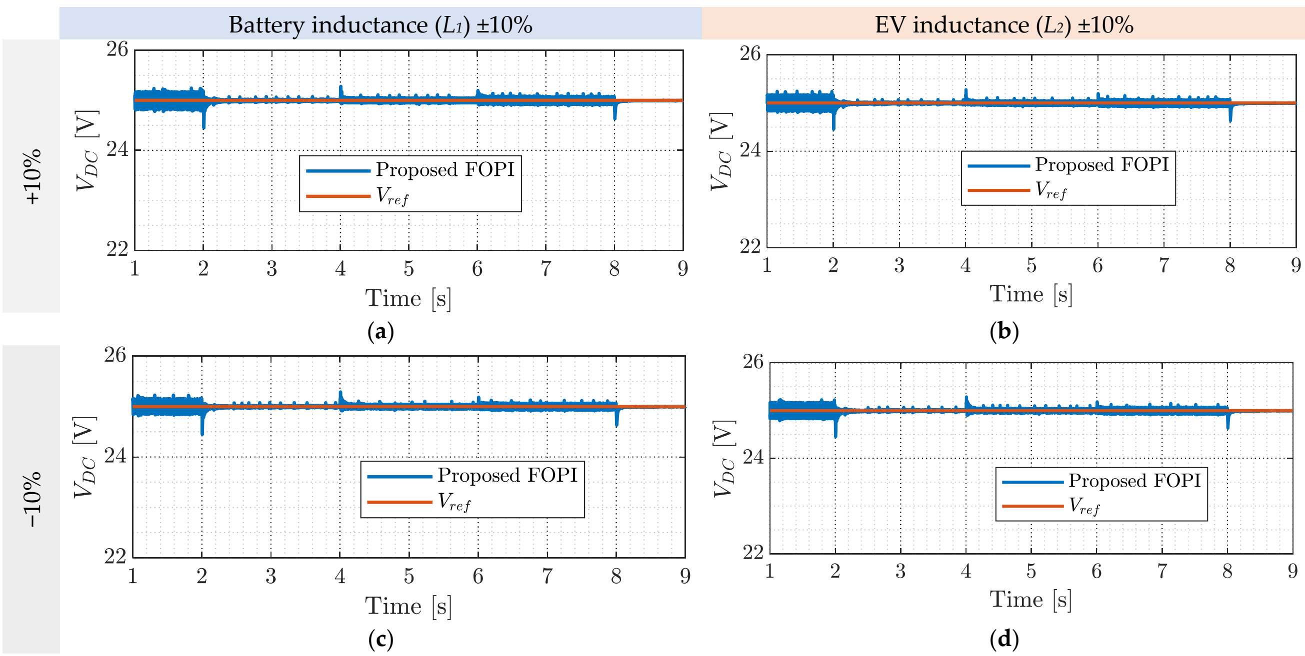

Figure 12. Effect of the (**a**,**c**) battery inductance (L_1) mismatch ±10% and (**b**,**d**) EV inductance (L_2) mismatch ±10% on the DC link voltage using the proposed FOPI controller.

Despite the merits of FOPI controllers compared to traditional PI controllers, they also come with certain limitations, such as complexity, tuning difficulty, limited industrial adoption, modeling challenges, and performance trade-offs. However, the last limitation is considered the main limitation of the proposed controller. Even though they can offer more flexibility, FOPI controllers may not necessarily perform better than conventional controllers in all circumstances. If not correctly tuned, the extra degrees of freedom in FOPI controllers might result in overfitting or inadequate performance. The recommended future work is the real-world implementation of the introduced system. The proposed power system has the advantage of simple scalability to the standard EVCS rating. Though many control software and hardware platforms are built around integer-order controllers like PID, FOPI controllers might not be readily supported in these systems. Hence, their integration and implementation are more challenging tasks.

6. Conclusions

The objective of this research paper is to introduce a new electric vehicle (EV) charging station that operates independently using a photovoltaic (PV) energy source. The proposed system is composed of several components, including a PV panel, boost converter, battery energy storage system (BESS), two DC/DC charging converters, and an EV battery. To ensure efficient operation, the control system encompasses three controllers: a maximum power point tracking (MPPT) controller, an EV charger controller, and a BESS controller. The battery controller utilizes the fractional-order technique in its dual loop control system to ensure a stable DC link voltage for the EV charger, even in the face of varying levels of sunlight. The grey wolf optimization (GWO) effectively achieved the desired optimal gains for the proposed FOPI controller. In order to test the effectiveness of the proposed EV charging station, a simulation using MATLAB/Simulink and the proposed optimal FOPI was conducted. The charging process of the EV battery remains stable regardless of the amount of sunlight, while the BESS effectively stores and compensates for variations in PV energy using the proposed optimal FOPI controller. Compared to the traditional PI controller, the proposed optimal FOPI controller reduces the voltage deviation of the DC link during changes in sunlight by approximately 8%. The converters' current and voltage controllers perform well and accurately follow their desired values. Moreover, the MPPT controller effectively monitors and adjusts to the optimal conditions of the PV system. In terms of future work, there is potential to further enhance the system by incorporating additional energy storage technologies. This would result in the development of hybrid distributed energy systems that facilitate the rapid charging of electric vehicles.

Author Contributions: Formal analysis and conceptualization were performed by S.A.Z.; modeling and controller tuning were assisted by A.B.; the article was evaluated and reviewed by H.A. (Hani Albalawi) and A.M.A.; and funding acquisition was aided by A.M.K. and H.A. (Hossam AbdelMeguid). All authors have read and agreed to the published version of the manuscript.

Funding: This research was funded by the Deputyship for Research and Innovation, Ministry of Education, Saudi Arabia through the University of Tabuk, grant number S-1443-0007.

Institutional Review Board Statement: Not applicable.

Informed Consent Statement: Not applicable.

Data Availability Statement: Not applicable.

Acknowledgments: The authors extend their appreciation to the Deputyship for Research and Innovation, Ministry of Education, Saudi Arabia for funding this research work through the project number (S-1443-0007).

Conflicts of Interest: The authors declare no conflict of interest.

References

1. Sun, X.; Li, Z.; Wang, X.; Li, C. Technology Development of Electric Vehicles: A Review. *Energies* **2020**, *13*, 90. [CrossRef]
2. Irle, R. Global EV Sales for the 1st Half of 2019. EV Volumes. 2019. Available online: http://www.ev-volumes.com/country/total-world-plug-in-vehicle-volumes/ (accessed on 20 November 2019).
3. Chakraborty, S.; Vu, H.-N.; Hasan, M.M.; Tran, D.-D.; Baghdadi, M.E.; Hegazy, O. DC-DC Converter Topologies for Electric Vehicles, Plug-in Hybrid Electric Vehicles and Fast Charging Stations: State of the Art and Future Trends. *Energies* **2019**, *12*, 1569. [CrossRef]
4. Luc, Vehicles & Charging Tips. Fastned. 2019. Available online: https://www.greencars.com/greencars-101/electric-car-charging-tips (accessed on 12 July 2023).
5. Minh, P.V.; Le Quang, S.; Pham, M.-H. Technical Economic Analysis of Photovoltaic-Powered Electric Vehicle Charging Stations under Different Solar Irradiation Conditions in Vietnam. *Sustainability* **2021**, *13*, 3528. [CrossRef]
6. Liu, Y.; Dong, H.; Wang, S.; Lan, M.; Zeng, M.; Zhang, S.; Yang, M.; Yin, S. An Optimization Approach Considering User Utility for the PV-Storage Charging Station Planning Process. *Processes* **2020**, *8*, 83. [CrossRef]
7. Francfort, J.; Salisbury, S.; Smart, J.; Garetson, T.; Karner, D. *Considerations for Corridor and Community DC Fast Charging Complex System Design*; Idaho National Lab: Idaho Falls, ID, USA, 2017.
8. Rafi, M.A.H.; Bauman, J. A Comprehensive Review of DC Fast Charging Stations with Energy Storage: Architectures, Power Converters, and Analysis. *IEEE Trans. Transp. Electrif.* **2021**, *7*, 345–368. [CrossRef]
9. Nicholas, M.; Hall, D. *Lessons Learned on Early Fast Electric Vehicle Charging Systems*; The National Academies of Sciences, Engineering, and Medicine: Washington, DC, USA, 2018.
10. Mouli, C.G.R.; Schijffelen, J.; Heuvel, M.; Kardolus, M.; Bauer, P. A 10 kW Solar-Powered Bidirectional EV Charger Compatible With Chademo and COMBO. *IEEE Trans. Power Electron.* **2019**, *34*, 1082–1098. [CrossRef]
11. Atawi, I.E.; Hendawi, E.; Zaid, S.A. Analysis and Design of a Standalone Electric Vehicle Charging Station Supplied by Photovoltaic Energy. *Processes* **2021**, *9*, 1246. [CrossRef]
12. Fathabadi, H. Novel grid-connected solar/wind powered electric vehicle charging station with vehicle-to-grid technology. *Energy* **2017**, *132*, 1–11. [CrossRef]
13. Awad, M.; Ibrahim, A.M.; Alaas, Z.M.; El-Shahat, A.; Omar, A.I. Design and analysis of an efficient photovoltaic energy-powered electric vehicle charging station using perturb and observe MPPT algorithm. *Front. Energy Res.* **2022**, *10*, 969482. [CrossRef]
14. Zhang, Y.; He, J.; Ionel, D.M. Modeling and control of a multiport converter based EV charging station with PV and battery. In Proceedings of the 2019 IEEE Transportation electrification conference and EXPO (ITEC), Detroit, MI, USA, 19–21 June 2019; pp. 1–5.
15. Singh, S.; Chauhan, P.; Singh, N.J. Feasibility of grid-connected solar-wind hybrid system with electric vehicle charging station. *J. Mod. Power Syst. Clean Energy* **2020**, *9*, 295–306. [CrossRef]
16. Ahmadi, M.; Kaleybar, H.J.; Brenna, M.; Castelli-Dezza, F.; Carmeli, M.S. DC Railway Micro Grid Adopting Renewable Energy and EV Fast Charging Station. In Proceedings of the 2021 IEEE International Conference on Environment and Electrical Engineering and 2021 IEEE Industrial and Commercial Power Systems Europe (EEEIC/I&CPS Europe), Bari, Italy, 7–10 September 2021; pp. 1–6.
17. Oulad-Abbou, D.; Doubabi, S.; Rachid, A.; García-Triviño, P.; Fernández-Ramírez, L.M.; Fernández-Ramírez, C.A.; Sarrias-Mena, R. Combined control of MPPT, output voltage regulation and capacitors voltage balance for three-level DC/DC boost converter in PV-EV charging stations. In Proceedings of the 2018 International Symposium on Power Electronics, Electrical Drives, Automation and Motion (SPEEDAM), Amalfi, Italy, 20–22 June 2018; pp. 372–376.
18. Traver, J.E.; Nuevo-Gallardo, C.; Tejado, I.; Fernández-Portales, J.; Ortega-Morán, J.F.; Pagador, J.B.; Vinagre, B.M. Cardiovascular Circulatory System and Left Carotid Model: A Fractional Approach to Disease Modeling. *Fractal Fract.* **2022**, *6*, 64. [CrossRef]
19. Muresan, C.I.; Birs, I.; Ionescu, C.; Dulf, E.H.; De Keyser, R. A Review of Recent Developments in Autotuning Methods for Fractional-Order Controllers. *Fractal Fract.* **2022**, *6*, 37. [CrossRef]
20. Yaghooti, B.; Hosseinzadeh, M.; Sinopoli, B. Constrained Control of Semilinear Fractional-Order Systems: Application in Drug Delivery Systems. In Proceedings of the IEEE Conference on Control Technology and Applications (CCTA), Montreal, QC, Canada, 24–26 August 2020; pp. 833–838. [CrossRef]
21. Saleem, O.; Ali, S.; Iqbal, J. Robust MPPT Control of Stand-Alone Photovoltaic Systems via Adaptive Self-Adjusting Fractional Order PID Controller. *Energies* **2023**, *16*, 5039. [CrossRef]
22. Zaid, S.A.; Bakeer, A.; Magdy, G.; Albalawi, H.; Kassem, A.M.; El-Shimy, M.E.; AbdelMeguid, H.; Manqarah, B. A New Intelligent Fractional-Order Load Frequency Control for Interconnected Modern Power Systems with Virtual Inertia Control. *Fractal Fract.* **2023**, *7*, 62. [CrossRef]
23. Bingi, K.; Prusty, R.; Singh, A. A Review on Fractional-Order Modelling and Control of Robotic Manipulators. *Fractal Fract.* **2023**, *7*, 77. [CrossRef]
24. Almasoudi, F.M.; Magdy, G.; Bakeer, A.; Alatawi, K.S.S.; Rihan, M. A New Load Frequency Control Technique for Hybrid Maritime Microgrids: Sophisticated Structure of Fractional-Order PIDA Controller. *Fractal Fract.* **2023**, *7*, 435. [CrossRef]
25. Oustaloup, A.; Levron, F.; Mathieu, B.; Nanot, F.M. Frequency-band complex noninteger differentiator: Characterization and synthesis. *IEEE Trans. Circuits Syst. I Fundam. Theory Appl.* **2000**, *47*, 25–39. [CrossRef]

26. Morsali, J.; Zare, K.; Hagh, M.T. Applying fractional order PID to design TCSC-based damping controller in coordination with automatic generation control of interconnected multi-source power system. *Eng. Sci. Technol. Int. J.* **2017**, *20*, 1–17. [CrossRef]
27. Mohamed, E.A.; Ahmed, E.M.; Elmelegi, A.; Aly, M.; Elbaksawi, O.; Mohamed, A.-A.A. An Optimized Hybrid Fractional Order Controller for Frequency Regulation in Multi-Area Power Systems. *IEEE Access* **2020**, *8*, 213899–213915. [CrossRef]
28. Salama, H.S.; Magdy, G.; Bakeer, A.; Vokony, I. Adaptive coordination control strategy of renewable energy sources, hydrogen production unit, and fuel cell for frequency regulation of a hybrid distributed power system. *Prot. Control. Mod. Power Syst.* **2022**, *7*, 34. [CrossRef]